Acta Pharmaceutica Sinica B 2025;15(2):722−736

Chinese Pharmaceutical Association
Institute of Materia Medica, Chinese Academy of Medical Sciences

Acta Pharmaceutica Sinica B

www.elsevier.com/locate/apsb
www.sciencedirect.com

ORIGINAL ARTICLE

Synthesis and evaluation of TSPO-targeting radioligand [^{18}F]F-TFQC for PET neuroimaging in epileptic rats

Wenhui Fu [a,b,c,†], **Qingyu Lin** [a,b,c,†], **Zhequan Fu** [a,b,c], **Tingting Yang** [a,b,c], **Dai Shi** [a,b,c], **Pengcheng Ma** [a,b,c], **Hongxing Su** [a,b,c], **Yunze Wang** [a,b,c], **Guobing Liu** [a,b,c], **Jing Ding** [d], **Hongcheng Shi** [a,b,c,*], **Dengfeng Cheng** [a,b,c,*]

[a]*Department of Nuclear Medicine, Zhongshan Hospital, Fudan University, Shanghai 200032, China*
[b]*Institute of Nuclear Medicine, Fudan University, Shanghai 200032, China*
[c]*Shanghai Institute of Medical Imaging, Shanghai 200032, China*
[d]*Department of Neurology, Zhongshan Hospital, Fudan University, Shanghai 200032, China*

Received 6 February 2024; received in revised form 15 April 2024; accepted 25 May 2024

KEY WORDS

Fluorine-18;
TSPO;
PET;
Epilepsy;
Neuroimaging

Abstract The translocator protein (TSPO) positron emission tomography (PET) can noninvasively detect neuroinflammation associated with epileptogenesis and epilepsy. This study explored the role of the TSPO-targeting radioligand [^{18}F]F-TFQC, an *m*-trifluoromethyl ER176 analog, in the PET neuroimaging of epileptic rats. Initially, [^{18}F]F-TFQC was synthesized with a radiochemical yield of 8%−10% (EOS), a radiochemical purity of over 99%, and a specific activity of 38.21 ± 1.73 MBq/nmol (EOS). After determining that [^{18}F]F-TFQC exhibited good biochemical properties, [^{18}F]F-TFQC PET neuroimaging was performed in epileptic rats at multiple time points in various stages of disease progression. PET imaging showed specific [^{18}F]F-TFQC uptake in the right hippocampus (KA-injected site, *i.e.*, epileptogenic zone), which was most pronounced at 1 week (T/NT 1.63 ± 0.21) and 1 month (T/NT 1.66 ± 0.20). The PET results were further validated using autoradiography and pathological analysis. Thus, [^{18}F]F-TFQC can reflect the TSPO levels and localize the epileptogenic zone, thereby offering the potential for monitoring neuroinflammation and guiding anti-inflammatory treatment in patients with epilepsy.

*Corresponding authors.
E-mail addresses: shi.hongcheng@zs-hospital.sh.cn (Hongcheng Shi), cheng.dengfeng@zs-hospital.sh.cn (Dengfeng Cheng).
†These authors made equal contributions to this work.

Peer review under the responsibility of Chinese Pharmaceutical Association and Institute of Materia Medica, Chinese Academy of Medical Sciences.

https://doi.org/10.1016/j.apsb.2024.05.031

1. Introduction

Neuroinflammation plays a key role in epileptogenesis and epilepsy, and patients with epilepsy may benefit from anti-inflammatory therapy[1]. The 18 kDa translocator protein (TSPO) is overexpressed in activated microglia and reactive astrocytes and has become a classic biomarker of neuroinflammation[2,3]. The development of TSPO positron emission tomography (PET) radioligands will aid in monitoring neuroinflammation, providing a basis for anti-inflammatory therapy, localizing the epileptogenic zone (EZ), and facilitating resective epilepsy surgery.

Numerous TSPO PET radioligands have been developed (Fig. 1). The first-generation radioligand [^{11}C]-(*R*)-PK11195 poses challenges in identifying subtle changes in the TSPO density owing to its low signal-to-noise ratio (SNR)[4]. Conversely, the second-generation radioligands (*e.g.*, [^{11}C]PBR-28, [^{11}C]DPA-713, and [^{18}F]DPA-714) have higher SNR but are sensitive to a single nucleotide polymorphism (rs6971)[5]. Gene polymorphisms result in three different binding abilities: high-affinity binding (HAB), mixed-affinity binding (MAB), and low-affinity binding (LAB). Therefore, the binding affinity of the second-generation TSPO radioligands varies among individuals, requiring genetic screening to exclude those with an LAB genotype[6]. The third-generation radioligands with fewer polymorphisms have also emerged, including [^{18}F]GE180, [^{18}F]GE387, [^{18}F]CB251, [^{18}F]BS224, [^{18}F]FEBMP, [^{18}F]LW223, [^{11}C]ER176, [^{18}F]BIBD-239, and [^{18}F]3b. However, [^{18}F]GE180 showed poor brain uptake and stability *in vivo*[7,8]. [^{18}F]GE387, developed based on the chemical scaffold of [^{18}F]GE180, also exhibits suboptimal stability[9,10]. [^{18}F]CB251 shows nonspecific uptake in the skull owing to defluorination, which hinders the exact quantification of TSPO expression[11]. [^{18}F]BS224 is a direct analog of [^{18}F]CB251 with favorable properties; however, only a few preclinical studies on [^{18}F]BS224 are currently available[12]. The stability of [^{18}F]FEBMP is poor, as radiometabolites increase rapidly to over 90% in rat plasma within 30 min[13,14]. [^{18}F]LW223 is difficult to purify, and its stability and pharmacokinetics *in vivo* require further verification[15]. [^{11}C]ER176 has a high SNR, exhibits low polymorphism sensitivity ($K_{i\ LABs/HABs}$ = 1.3), and does not generate brain-penetrant radiometabolites, making it the preferred TSPO radioligand[16,17]. Meanwhile, [^{11}C]ER176 is the only third-generation radioligand that has undergone Phase III clinical trials (NCT04762719). However, ^{11}C-labeled tracers have a relatively short half-life of carbon-11 (C-11, $t_{1/2}$ = 20.4 min). By contrast, fluorine-18 (F-18, $t_{1/2}$ = 109.8 min) is the most widely used PET radionuclide, which can be produced in larger doses at once and can be transported over longer distances. Thus, [^{18}F]BIBD-239 was recently synthesized by introducing fluorine atoms into the aliphatic side chain of the ER176 terminal group[18]. However, the stability of [^{18}F]BIBD-239 must be improved. Lee et al.[19] have synthesized and evaluated six ER176 fluorine-containing analogs labeled with C-11, of which the *m*-trifluoromethyl analog of ER176 (SF12057) exhibited the highest SUV_{peak} (3.4) and high BP_{ND} (11.7) in the monkey brain. Considering that labeling SF12057 with F-18 requires great efforts to optimize specific activity and achieve automated production, Siméon et al.[20] turned

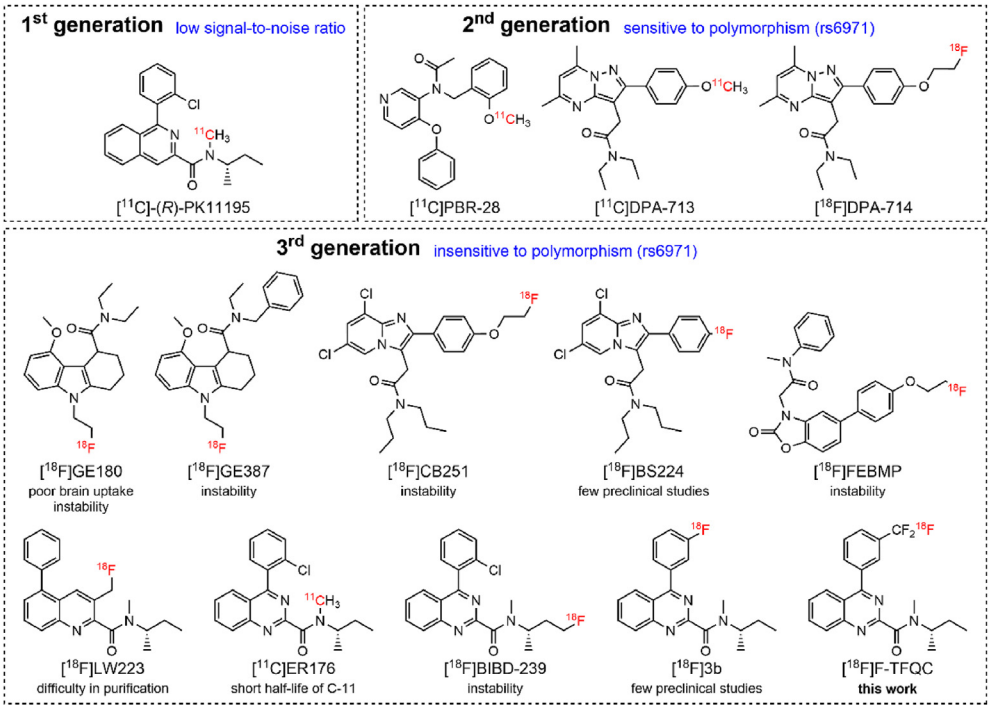

Figure 1 Representative TSPO-targeting PET radioligands.

to label *m*-fluoro analog with F-18 ([^{18}F]3b). However, further preclinical evaluation of [^{18}F]3b is warranted.

Notably, the *m*-trifluoromethyl ER176 fluoride has excellent properties (rat kidney K_i = 1.44 nmol/L, human U87MG K_i = 1.19 nmol/L, *c*log*D* = 3.30, log$D_{7.4}$ = 3.71, low sensitivity to the TSPO genotype with a $K_{i\ LABs/HABs}$ of 1.98) and it is highly suitable for labeling with F-18[19,20]. In this study, we aimed to synthesize precursor Ar-CF_2Br from Ar-$CF_2SO_2CF_3$ and subsequently label it with F-18 to obtain the *m*-trifluoromethyl ER176 radioligand. Further, the role of the prepared radioligand in monitoring neuroinflammation and visualizing EZ in epileptic rat models using PET neuroimaging was explored.

2. Results and discussion

2.1. Chemistry and radiochemistry

Compared with C-11 ($t_{1/2}$ = 20.4 min), F-18 with a longer half-life ($t_{1/2}$ = 109.8) is more appropriate for complex radiosynthesis and long-distance transportation. In addition, the suitable energy (0.635 MeV) of F-18 helps us obtain PET images with higher resolution. As ER176 does not contain a fluorine atom that allows for labeling with F-18, six new fluorine-containing ER176 derivatives were developed and evaluated by Lee et al.[19], and Siméon et al.[20] Among these six ER176 fluorides, *m*-trifluoromethyl compound has the highest affinity (rat kidney K_i = 1.44 nmol/L, human U87MG K_i = 1.19 nmol/L), suitable lipophilicity (*c*log*D* = 3.30, log$D_{7.4}$ = 3.71), and low sensitivity to the TSPO genotype (*in vitro* $K_{i\ LABs/HABs}$ of 1.98)[19,20]. The *m*-trifluoromethyl ER176 analog has become one of the best candidates for radiolabeling with F-18. Considering that labeling **3e** (*m*-trifluoromethyl) with F-18 requires extra effort to optimize the specific activity and achieve automated production, Siméon et al.[20] only selected **3b** (*m*-fluoro) for labeling with F-18. To date, several methods have been used to label Ar-CF_3 with F-18, including the halogen exchange of Ar-CF_2X (X = F, Cl, Br, and I) with [^{18}F]F$^-$[21], [^{18}F]fluorodecarboxylation of Ar-CF_2COOH using [^{18}F]Selectfluor[22], copper-mediated [^{18}F]trifluoromethylation of aryl boronic acids and aryl iodides[23,24], and direct C−H [^{18}F]trifluoromethylation using [^{18}F]$CF_3SO_2NH_4$[25]. Current strategies either lack operational simplicity or broad applicability, hindering clinical translation[26]. The [^{18}F]trifluoromethylation of aryl boronic acids and aryl iodides has been reported to be highly efficient and has previously been used for radiosynthesis of [^{18}F]F-PTTP in our laboratory[27]. However, the radiochemical yield (RCY) of [^{18}F]F-PTTP is not satisfactory, and operationally simple radiofluorination conditions are still required. Compounds containing a CF_2Br group have been widely used as radiolabeling precursors[28-31]. Moreover, labeling the Ar-CF_2Br precursor with F-18 is a facile and widely adopted method[21,30,31]. Hence, **3e** was labeled with F-18 using this approach in our study. We first synthesized Pre-CF_3-1 from the commercially available isatoic anhydride in 1 step (Scheme 1). Then, Pre-CF_2-QC was synthesized with the trifluoromethylsulfonyl group (−SO_2CF_3) from Pre-CF_3-1 in 9 steps. −SO_2CF_3 is a relatively bulky and strong electron-withdrawing group, which could produce strong steric and static repulsions between two α-fluorine atoms and −SO_2CF_3[21]. Therefore, we obtained the precursor Br-CF_2-QC for radiolabeling via the cleavage of the −SO_2CF_3 of Pre-CF_2-QC with a total yield of 0.38% (Scheme 2), which was confirmed by electrospray ionization-mass spectrometry (ESI-MS), ^{1}H nuclear magnetic resonance (NMR) and ^{19}F NMR. In addition, [^{19}F]F-TFQC was synthesized starting from Pre-CF_3-1 in 3 steps with a total yield of 2.10% (Scheme 3). The ^{1}H, ^{13}C, and ^{19}F NMR and ESI-MS spectra of the synthesized [^{19}F]F-TFQC were identical to the previously reported data[20]. The intermediate compounds and final products were characterized using ^{1}H, ^{19}F, and ^{13}C NMR, or ESI-MS. Details of the results are presented in the Experimental section and Supporting Information.

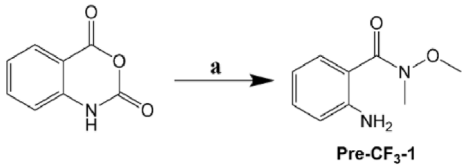

Scheme 1 Reagents and conditions: (a) isatoic anhydride, DMHH, DMAP, Et_3N, ACN, RT, 24 h, 81.31%.

The precursor Br-CF_2-QC was successfully labeled with [^{18}F]F$^-$ to synthesize [^{18}F]F-TFQC using a one-pot nucleophilic substitution method (Scheme 4). [^{18}F]F-TFQC was identified by the co-injection of [^{18}F]F-TFQC and [^{19}F]F-TFQC into an analytical radio-high performance liquid chromatography (HPLC) (Fig. 2). The radiosynthesis of [^{18}F]F-TFQC required 84.0 ± 5.2 min and obtained an RCY of 8%−10%, which was decay-corrected to the end of synthesis (EOS); a radiochemical purity (RCP) of more than 99% and a specific activity of 38.21 ± 1.73 MBq/nmol (EOS). Building upon the work of Lee et al.[19] and Siméon et al.[20], significant advancements have been made in the successful radiosynthesis of [^{18}F]F-TFQC, achieving a moderate specific activity and enabling automated production. In addition, Zhang et al.[30] and Huang et al.[31] successfully prepared [^{18}F]GSK1482160 using the same radiosynthesis method. In this study, the RCY and specific activity of the [^{18}F]F-TFQC were only slightly lower than those of [^{18}F]GSK1482160, which is possibly attributed to the automated production. In summary, [^{18}F]F-TFQC can fully meet the requirements of preclinical and clinical studies. Nevertheless, further enhancements can still be made to increase the RCY (8%−10%, EOS).

2.2. In vitro and in vivo stabilities, octanol/water partition coefficient, in vitro cell binding assay, and immunocytochemistry

First, the *in vitro* stability of [^{18}F]F-TFQC was tested. Results showed [^{18}F]F-TFQC was stable in both normal saline (NS) and 0.1% bovine serum albumin (BSA), with more than 99% of the parent compound present after 6 h of incubation (Fig. 3A). Furthermore, the *in vivo* stability experiment was conducted. It showed that [^{18}F]F-TFQC was stable in the brain with 98% of the parent compound remaining in 60 min (Fig. 3B). The octanol/water partition coefficient was 1.41 ± 0.01, suggesting that [^{18}F]F-TFQC has reasonable lipophilicity (log*P* 1−3 for central nervous system radioligand) and the potential to penetrate the brain for neuroimaging[32]. The [^{18}F]F-TFQC uptake in RAW 264.7 cells could be blocked by the addition of excessive amounts of [^{19}F]F-TFQC with a good blocked effect (74.77 ± 1.28%) at 2 h ($P < 0.001$), suggesting the high cellular specificity of [^{18}F]F-TFQC (Fig. 3C). In addition, [^{18}F]F-TFQC maintained a potent targeting affinity for TSPO (apparent K_d ∼13.30 nmol/L, apparent B_{max} ∼4.27 × 10^{-9} mol/cell) on RAW 264.7 cells

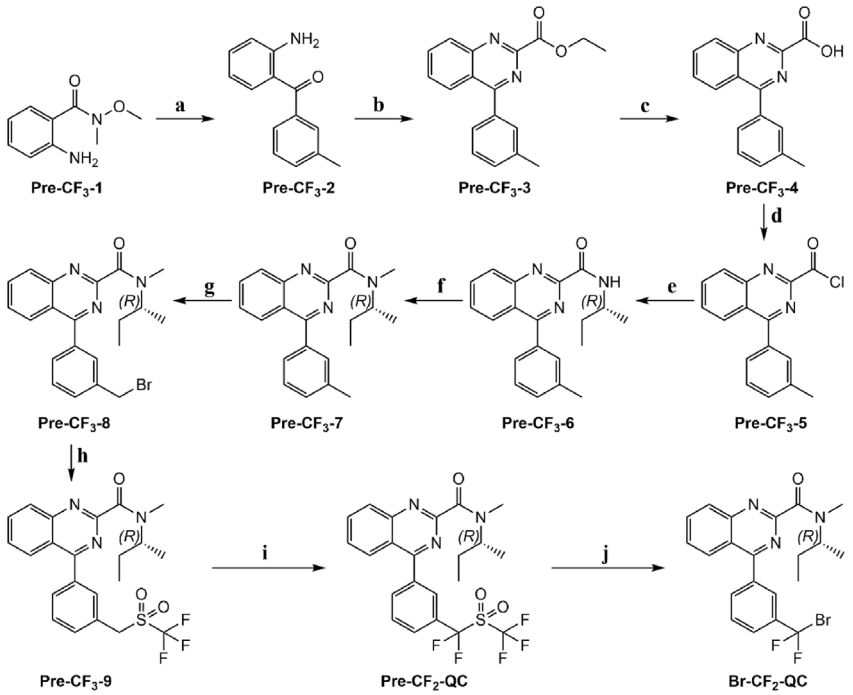

Scheme 2 Reagents and conditions: (a) 3-bromotoluene, *n*-BuLi, THF, RT, 24 h, 44.47%; (b) ethyl glyoxalate, NH_4OAc, RT, 72 h, 37.16%; (c) NaOH, EtOH, RT, 24 h, 79.03%; (d) OC, DCM, DMF, 74.02%; (e) (*R*)-(−)-2-aminobutane, Et_3N, DCM, RT, 2 h, 86.03%; (f) *t*-BuOK, THF, CH_3I, RT, 16 h, 64.29%; (g) NBS, AIBN, DCE, 80 °C, 16 h, 53.03%; (h) CF_3SO_2Na, ACN, 80 °C, 16 h, 84.71%; (i) NFSI, K_3PO_4, DMF, RT, 16 h, 35.66%; (j) LiBr, ACN, 80 °C, 16 h, 55.00%.

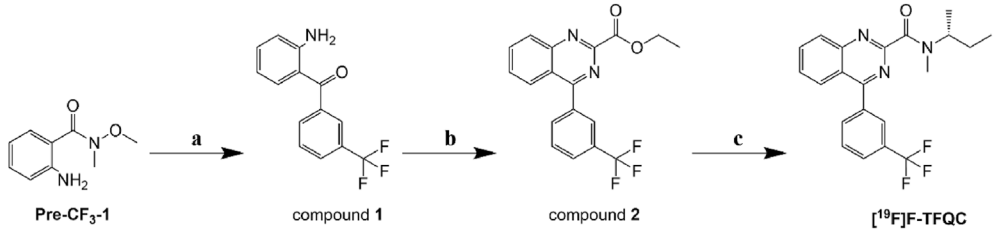

Scheme 3 Reagents and conditions: (a) 3-bromobenzotrifluoride, *n*-BuLi, THF, −30 °C, 2 h, 22.22%; (b) ethyl glyoxalate, NH_4OAc, RT, 3 days, 23.26%; (c) trimethylaluminium, (*R*)-(−)-2-aminobutane, DCE, 80 °C, 2 h, 50.00%.

(Fig. 3D). At the same time, the immunocytochemistry (ICC) analysis (Fig. 3E and F) confirmed the TSPO overexpression in RAW 264.7 cells. In summary, [^{18}F]F-TFQC exhibited sufficient stability, high specificity, and high affinity for use in further experiments.

2.3. *Biosafety*

To examine the toxicity of [^{18}F]F-TFQC, we observed mice from the NS, low-dose (3.7 MBq/0.1 nmol), medium-dose (18.5 MBq/0.5 nmol), and high-dose (37 MBq/1.0 nmol) groups for 4 weeks after NS or [^{18}F]F-TFQC injection. Hematological examinations, including white blood cell count (WBC), red blood cell count (RBC), platelet count (PLT), alanine aminotransferase (ALT), aspartate aminotransferase (AST), albumin (ALB), urea (UREA), creatinine (CREA), and uric acid (UA), were performed on these mice at the end of the observation period. For the NS, low-dose, medium-dose, and high-dose groups, no significant difference was found between these hematological indicators ($P > 0.05$) (Fig. 4A), no significant difference was observed between the body weights at different time points ($P > 0.05$) (Fig. 4B), and no evident cell necrosis or structural disorders were noted in H&E staining of multiple organs (Fig. 5). In summary, [^{18}F]F-TFQC showed no apparent toxicity or adverse effects.

2.4. *Pharmacokinetics and biodistribution*

To observe the radiometabolism and distribution of [^{18}F]F-TFQC, *in vivo* pharmacokinetics and *ex vivo* biodistribution experiments were conducted in healthy mice (Fig. 6). The *in vivo* blood half-life values of [^{18}F]F-TFQC were $t_{1/2\alpha}$ ~7.89 min and $t_{1/2\beta}$ ~76.97 min (Fig. 6A). The biodistribution data (Fig. 6B)

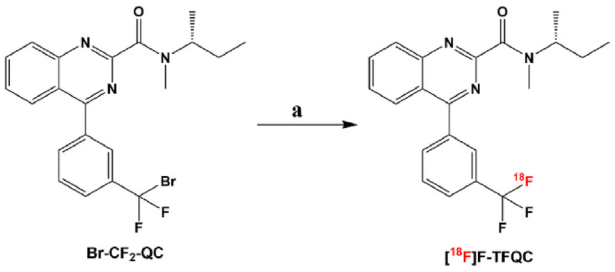

Scheme 4 Reagents and conditions: (a) [^{18}F]TEAB, ACN, 120 °C, 15 min, RCY 8%−10% (EOS).

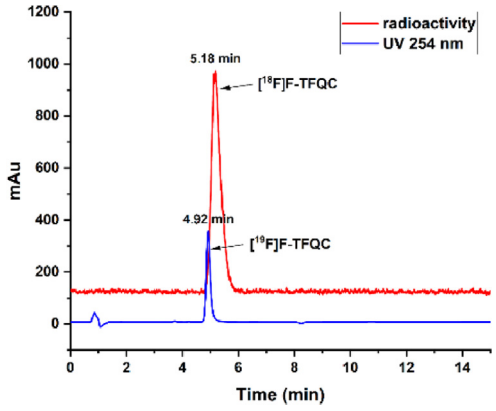

Figure 2 Radio-HPLC chromatogram from co-injection of [^{18}F]F-TFQC and [^{19}F]F-TFQC. Conditions: mobile phase, 5.5/4.5 (*v*/*v*) ACN/H_2O (containing 0.1% TFA); flow rate, 1 mL/min.

revealed a remarkably high uptake of [^{18}F]F-TFQC in the lung (23.02 ± 1.15% ID/g, 15 min post injection) related to the strong TSPO expression. Still, it rapidly decreased (3.12 ± 0.48% ID/g, 4 h post injection). In addition, the increased uptake of [^{18}F]F-TFQC also occurred in the heart, kidney, spleen, liver, stomach, and intestine, with relatively low distribution in other tissues. The [^{18}F]F-TFQC uptake in the brain was low (<0.8% ID/g) during the study period and decreased over time due to the minimal expression of TSPO in the healthy brains. From 15 min to 4 h post injection, the bone uptake remained between 0.57% and 0.95% ID/g without a significant increase, suggesting that there was only a tiny amount of defluorination of [^{18}F]F-TFQC. This finding aligns with the inherent stability of the trifluoromethyl, which exhibits relatively low susceptibility to defluorination and degradation[33].

2.5. *Micro PET/CT imaging in epileptic rats*

To further evaluate the applicability of [^{18}F]F-TFQC in assessing epilepsy, we performed micro PET/CT on rats at 1 day (sham, $n = 6$; epilepsy, $n = 10$), 1 week (sham, $n = 6$; epilepsy, $n = 13$), and 1 month (sham, $n = 6$; epilepsy, $n = 13$) after surgery. Subsequently, PET and magnetic resonance imaging (MRI) images were overlaid to obtain the precise mapping of the radioligand in rat brains. The volume of interests (VOIs) for "Hippocampus" were outlined based on the rat (W. Schiffer) atlas of the PMOD 3.2 software (Fig. 7A). The time−activity curves (TACs) of the hippocampus were generated by delineating the VOIs. The radioactivity in the epilepsy group was significantly higher than that in the sham group (area under curve: 9294 ± 365.6 *vs.* 4793 ± 83.43, $P < 0.05$) (Fig. 7B). The radioactivity in the right hippocampus rapidly increased with a peak of mean standard uptake values (SUV_{mean}) of 3.3, which was comparable to the SUV_{peak} (3.4) of the ^{11}C-labeled *m*-trifluoromethyl radioligand in the monkey brain[19]. In addition,

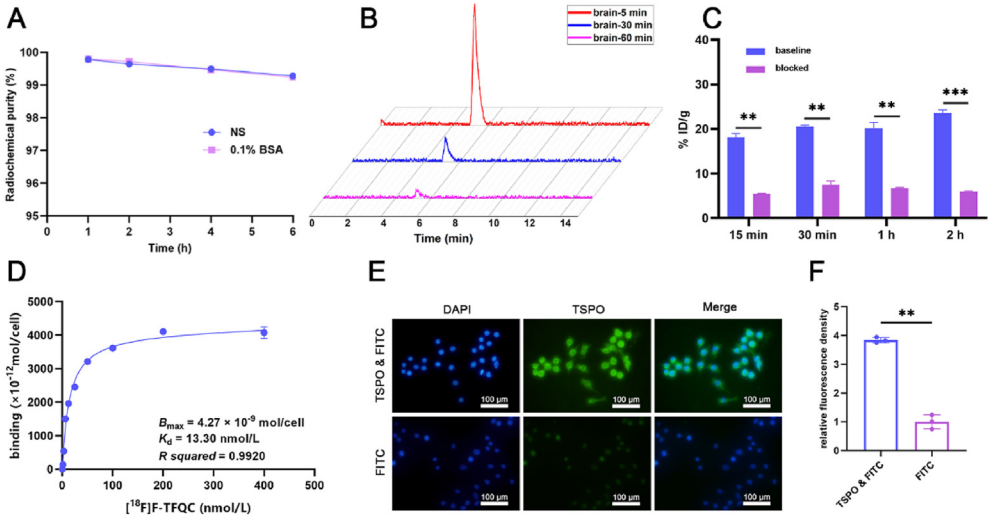

Figure 3 (A) *In vitro* stability of [^{18}F]F-TFQC in both NS and 0.1% BSA (radiochemical purity >99%). NS: normal saline, BSA: bovine serum albumin. (B) *In vivo* stability of [^{18}F]F-TFQC in the brain (radiochemical purity >98%). (C) The binding specificity assay of [^{18}F]F-TFQC in RAW 264.7 cells (blocked 74.77 ± 1.28% at 2 h, $P < 0.001$). % ID/g: percentage of injected dose per gram. $^{**}P < 0.01$, $^{***}P < 0.001$, paired *t*-test. (D) RAW 264.7 cell saturation binding of [^{18}F]F-TFQC (apparent K_d ~13.30 nmol/L, apparent B_{max} ~4.27×10^{-9} mol/cell). (E, F) ICC images and quantitative analysis indicated TSPO overexpression on RAW 264.7 cells (40 ×, scale bar = 100 μm). $^{**}P < 0.01$, paired *t*-test. Data are presented as mean ± standard deviation.

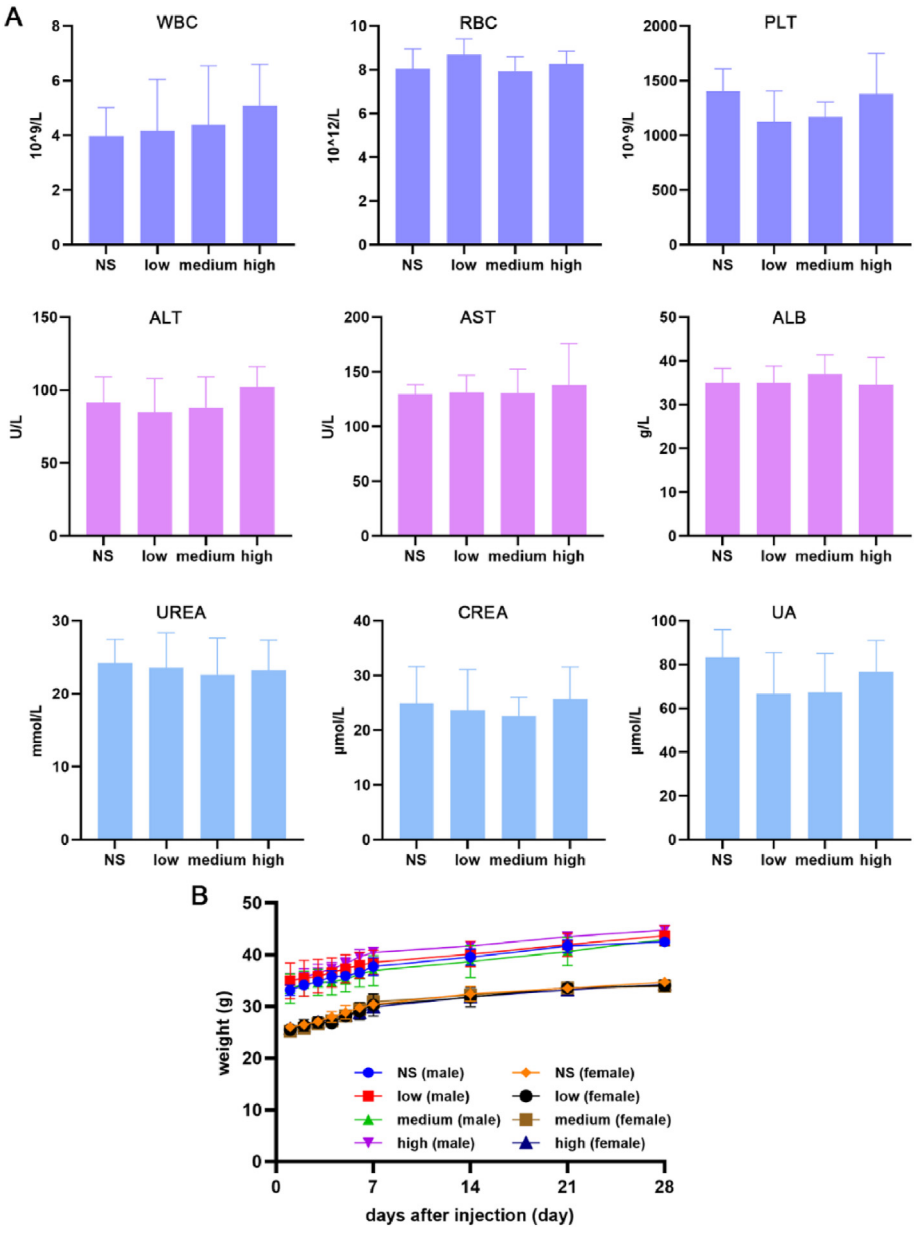

Figure 4 (A) Hematological examinations performed on healthy mice 4 weeks after NS or [18F]F-TFQC administration, including blood routine (WBC, RBC, and PLT), liver function (ALT, AST, and ALB), and kidney function (UREA, CREA, and UA) tests. (B) The weight of mice at different time points during 28 days. NS: normal saline, low: 3.7 MBq/0.1 nmol of [18F]F-TFQC, medium: 18.5 MBq/0.5 nmol of [18F]F-TFQC, high: 37 MBq/1.0 nmol of [18F]F-TFQC. Data are presented as mean ± standard deviation.

[18F]F-TFQC has a TAC similar to that of the 11C-labeled *m*-trifluoromethyl radioligand, which shows a rapid decrease followed by a slow clearance of radioactivity[19]. The fusion images of PET and MRI templates of epileptic rat models from 0 to 60 min indicated radioactivity in the right hippocampus (*i.e.*, EZ), which was blocked by excessive amounts of [19F]F-TFQC ($n = 3$) (Fig. 7C and D, $P < 0.05$). Notably, kainic acid (KA)-induced epilepsy models have been widely used in temporal lobe epilepsy studies, and electroencephalogram shows seizures typically originate from the KA-injected hippocampus[34,35]. Based on previous well-established studies, the KA-injected site (*i.e.*, the right hippocampus) was considered to be the EZ. The specific uptake of [18F]F-TFQC in the right hippocampus provides potential evidence support for the EZ localization. The images summed from 45 to 60 min revealed [18F]F-TFQC uptake in EZ differed during different periods (Fig. 7E and F). The uptake of [18F]F-TFQC in the right hippocampus was significantly higher in the epilepsy group than in the sham group, especially at 1 week (T/NT 1.63 ± 0.21 *vs.* 0.99 ± 0.08, $P < 0.001$) and 1 month (T/NT: 1.66 ± 0.20 *vs.* 0.99 ± 0.03, $P < 0.001$) after surgery, suggesting prolonged neuroinflammation in epilepsy. Epilepsy is a complex disorder associated with TSPO, and epilepsy models are required for advancing scientific research. Several epilepsy models have been

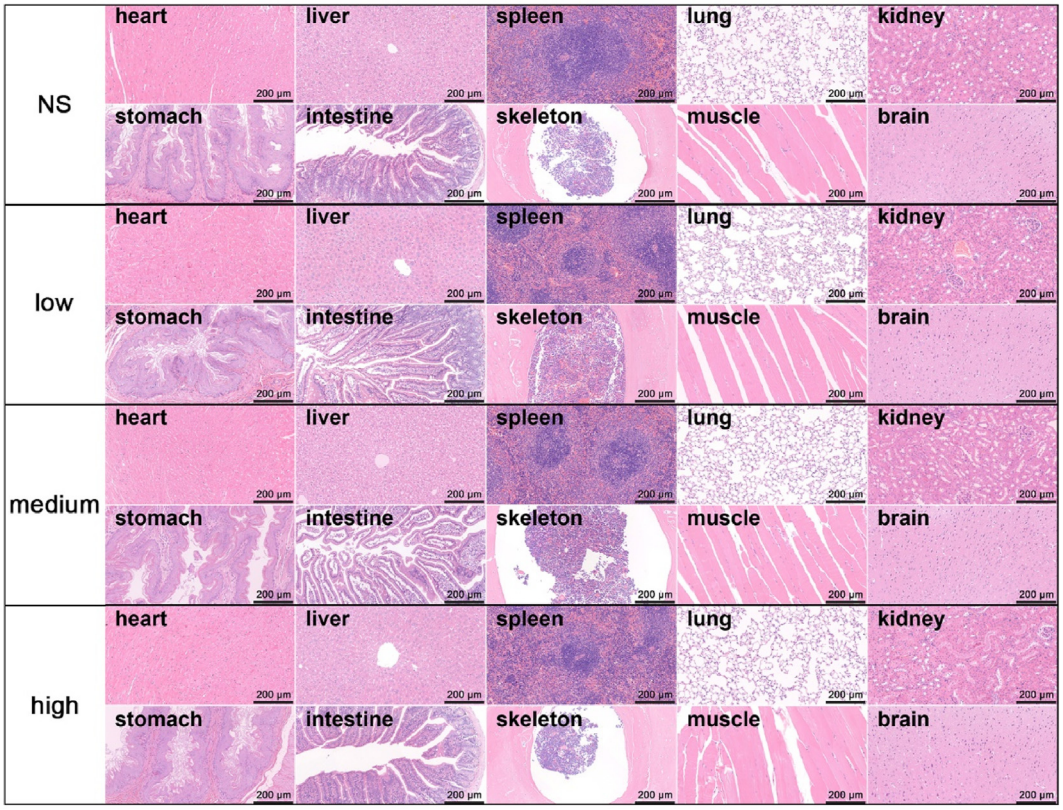

Figure 5 H&E staining (20 ×, scale bar = 200 μm) of heart, liver, spleen, lung, kidney, stomach, intestine, skeleton, muscle, and brain of mice in the NS, low-dose, medium-dose, and high-dose groups, with no observed cell necrosis or structural disorders. NS: normal saline, low: 3.7 MBq/0.1 nmol of [^{18}F]F-TFQC, medium: 18.5 MBq/0.5 nmol of [^{18}F]F-TFQC, high: 37 MBq/1.0 nmol of [^{18}F]F-TFQC.

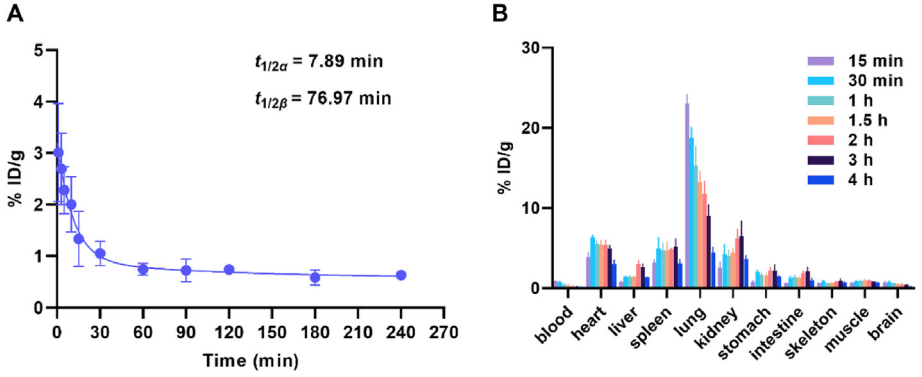

Figure 6 (A) Blood pharmacokinetics of [^{18}F]F-TFQC in healthy mice ($t_{1/2\alpha}$ ~7.89 min; $t_{1/2\beta}$ ~76.97 min). (B) Biodistribution of [^{18}F]F-TFQC in healthy mice (high uptake in the lung, heart, kidney, spleen, liver, stomach, and intestine, with low distribution in other tissues). % ID/g: percentage of injected dose per gram.

reported[36], and the KA model is frequently employed. The intracerebral administration of KA offers focal precision. Therefore, Sprague−Dawley (SD) rats were selected for KA injection into the hippocampal CA1 region to achieve a precise intervention and reduce mortality. The epilepsy models underwent PET neuroimaging, and PET images were analyzed. However, PET image analysis necessitates a reference region. The cerebellum can be used as the reference region for TSPO quantitative analysis[37]. As is commonly understood, epilepsy models can profoundly affect the temporal lobe, thalamus, cerebellum, and other areas, resulting in pathological changes[38,39]. Therefore, the "CaudatePutmen" was selected as the reference region owing to its relatively low radioactivity distribution. Nonetheless, more suitable methods for data analysis, such as the arterial input function (AIF), must be developed. AIF helps to accurately qualify the PET data, especially in the absence of a reference region. However, measuring the AIF in rodents is challenging owing to their small total blood volume and the

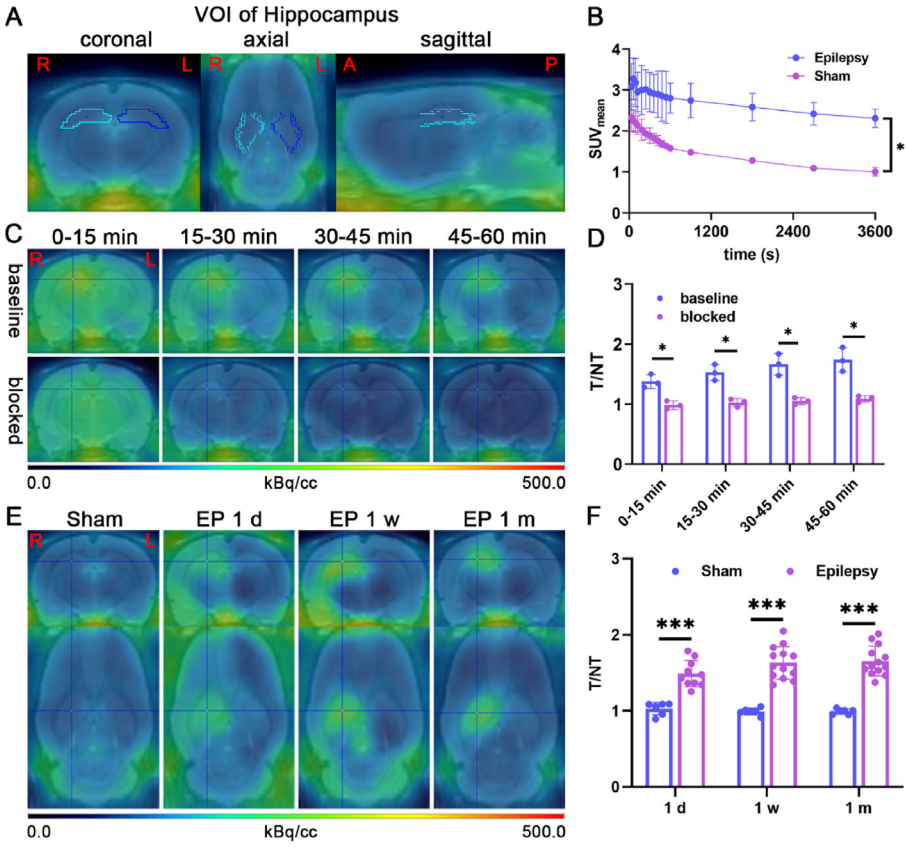

Figure 7 (A) The VOIs of "Hippocampus" were delineated based on the rat (W. Schiffer) atlas of PMOD 3.2 software. R: right, L: left, A: anterior, P: posterior. (B) The TACs of the right "Hippocampus" were generated based on the VOIs of the right "Hippocampus" (KA- or NS-injected site). *$P < 0.05$, paired *t*-test. (C) The fusion images of PET and MRI templates at different time points between baseline and blocked epileptic rats. Baseline: [^{18}F]F-TFQC, blocked: 2 mg/kg [^{19}F]F-TFQC 10 min prior [^{18}F]F-TFQC administration. The blue crosses indicate the KA-injected site of the right hippocampus, *i.e.*, epileptogenic zone. (D) T/NT values at different time points between baseline and blocked epileptic rats. T/NT: $SUV_{mean(Hippocampus)}/SUV_{mean(CaudatePutmen)}$. *$P < 0.05$, paired *t*-test. (E) The fusion images of PET (45−60 min) and MRI templates between sham and epileptic rats. (F) T/NT values between sham and epileptic rats. ***$P < 0.001$, independent sample *t*-test. Data are presented as mean ± standard deviation.

difficulties associated with blood collection[40]. Ongoing efforts are focused on developing effective methods to overcome this difficulty.

2.6. *In vitro autoradiography*

To accurately localize and confirm the specificity of [^{18}F]F-TFQC for TSPO, we performed autoradiography on rat brain slices. The baseline image of the sham groups showed diffuse mild signals (Fig. 8A), which disappeared after incubation with excessive amounts of PK11195 (14.17 μmol/L) or [^{19}F]F-TFQC (12.91 μmol/L) (both $P < 0.001$) (Fig. 8B). In the sham group, focal signals of the left cortex in the baseline image were caused by inadequate cleaning during the experiment. Epilepsy brain slices showed substantially increased focal signals in the right hippocampus (*i.e.*, EZ) (Fig. 8C) that could be blocked by excessive amounts of PK11195 (14.17 μmol/L) or [^{19}F]F-TFQC (12.91 μmol/L) (both $P < 0.01$) (Fig. 8D). These results indicated that EZ in epileptic rats can specifically accumulate [^{18}F]F-TFQC. Notably, the baseline image of the epilepsy brain slice showed focal signals in the left hippocampus, which may have been caused by seizures on the affected side involving the contralateral hippocampal region.

2.7. *Pathology*

Nissl staining revealed a loss of neuronal cells in the CA1, CA3, and DG regions of the right hippocampus in the epilepsy group (Fig. 9A). In particular, the CA1 ($P < 0.001$) and CA3 ($P < 0.001$) areas of the hippocampus in the epilepsy group were severely necrotic, showing a chaotic cell arrangement and undefined edges. By contrast, the hippocampal cells in the sham group showed no evident necrosis (Fig. 9B). Severe neuronal loss occurred in the CA1 region owing to the injection of KA into this region. GluK4 and GluK5, two KA receptor subunits with high affinity for KA, are mainly concentrated in the CA3[36]. This might explain the pattern of excitotoxic damage in this region and suggests that they are likely responsible for neuronal cell death. Our experimental results from our KA-induced epilepsy model are consistent with this fact. Immunohistofluorescence (IHF) staining of the right hippocampus in the sham and epilepsy groups at different periods showed increased expression of TSPO, CD68 (an activated microglia biomarker), and GFAP (an astrocytes biomarker) (Fig. 9C). This phenomenon was particularly evident in the CA3 region (Fig. 9D). The changing pattern of TSPO expression was consistent with the [^{18}F]F-TFQC uptake on PET imaging, indicating that PET neuroimaging with [^{18}F]F-TFQC is a

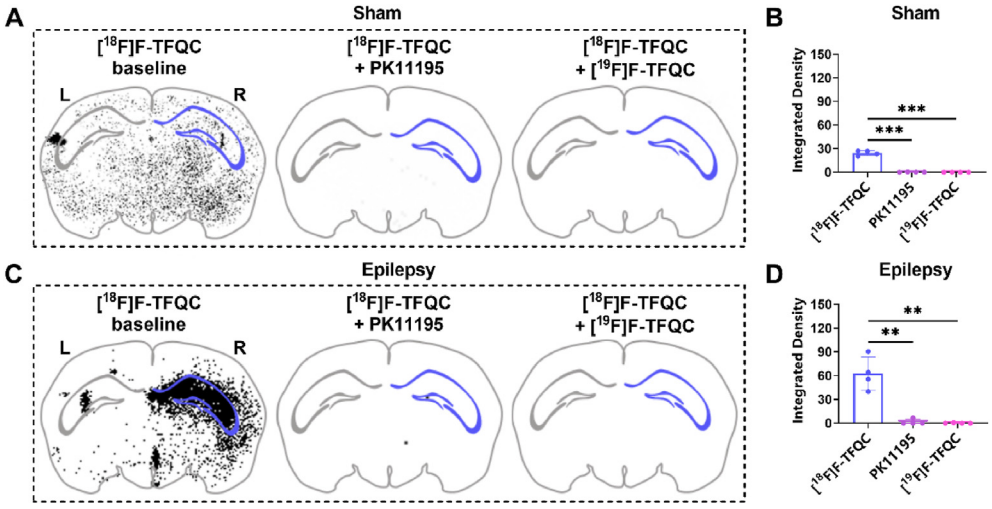

Figure 8 (A, B) Autoradiography of [^{18}F]F-TFQC in sham rat brain slices showed mild signals, which could be blocked by excessive amounts of PK11195 (14.17 μmol/L) and [^{19}F]F-TFQC (12.91 μmol/L). ***$P < 0.001$, paired *t*-test. (C, D) Autoradiography of [^{18}F]F-TFQC in epilepsy rat brain slices indicated strong signals in the right hippocampus, which disappeared after incubation with excessive amounts of PK11195 (14.17 μmol/L) and [^{19}F]F-TFQC (12.91 μmol/L). **$P < 0.01$, paired *t*-test. R, right; L, left; the regions outlined by the blue line represent the right hippocampus. Data are presented as mean ± standard deviation.

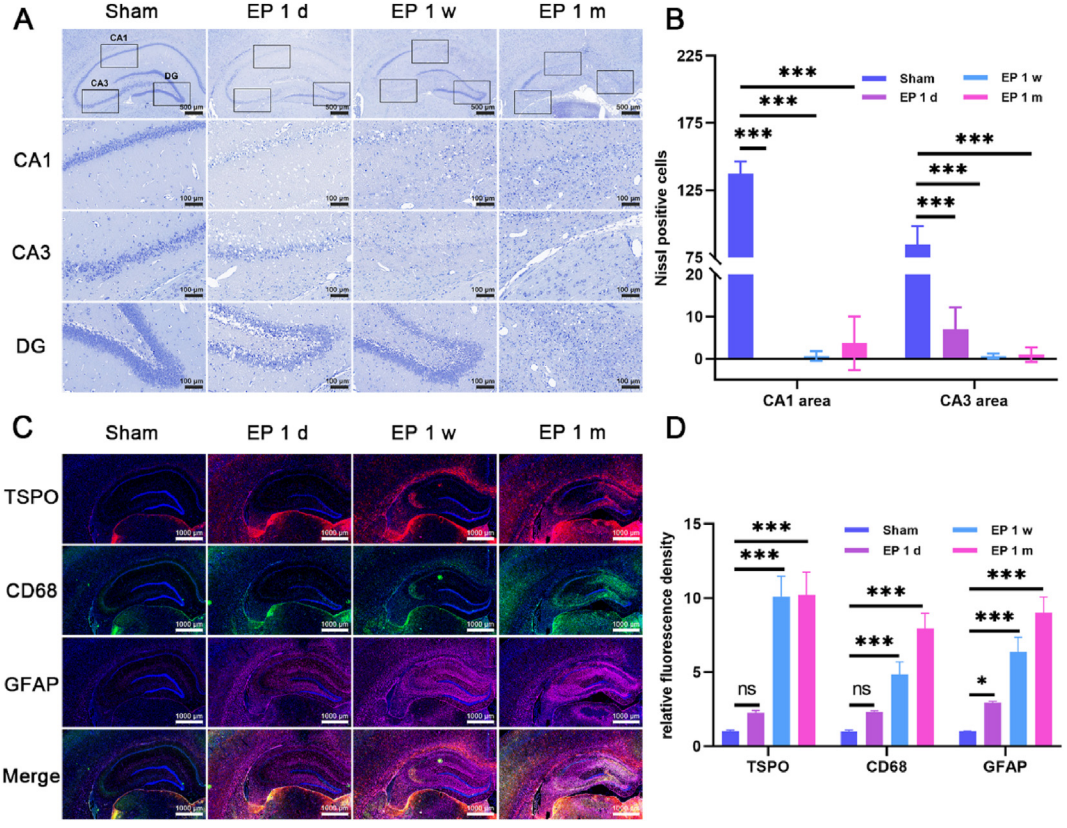

Figure 9 (A) Nissl staining images of the sham and epilepsy groups at different periods. The first row shows the right hippocampus (20 × , scale bar = 500 μm), while the following three rows show the CA1, CA3, and DG regions of the right hippocampus, respectively (100 × , scale bar = 100 μm). (B) The number of the Nissl^{+} cells (neuronal cells) in the CA1 and CA3 areas of the right hippocampus in the epilepsy groups was less than that in the sham group. ***$P < 0.001$, paired *t*-test. (C) IHF staining of the right hippocampus in the sham and epilepsy groups at different periods (150 × , scale bar = 1000 μm). The TSPO, CD68, and GFAP expression increased in the epilepsy group, especially in the CA3 area. (D) The relative fluorescence intensity of TSPO, CD68, and GFAP in the epilepsy group was stronger than that in the sham group. ns: $P > 0.05$, *$P < 0.05$, ***$P < 0.001$, paired *t*-test. Data are presented as mean ± standard deviation.

valuable tool for the quantification and visualization of TSPO and monitoring neuroinflammation. Furthermore, IHF results revealed a continual increase in the activation of the CD68 for 1 month, which may be related to transient microglial activation induced by frequent spontaneous recurrent seizures in rat models. Moreover, the GFAP expression increased, which is consistent with the pathological results of hippocampal sclerosis caused by epilepsy. In summary, the increased expression of TSPO, CD68, and GFAP suggests persistent or recurrent neuroinflammation during epileptogenesis.

3. Conclusions

In this study, a novel TSPO-targeting radioligand [^{18}F]F-TFQC was designed and synthesized for PET neuroimaging. This radioligand achieved automated production through a nucleophilic substitution reaction and possessed good biochemical properties. Moreover, [^{18}F]F-TFQC PET neuroimaging can noninvasively visualize TSPO levels, monitor neuroinflammation, and localize EZ in epileptic rats, thus facilitating the development of anti-inflammatory drugs, providing a basis for anti-inflammatory treatment, and guiding resective epilepsy surgery.

4. Experimental

4.1. Reagents, instruments, and animals

The Br-CF_2-QC, [^{19}F]F-TFQC, and [^{18}F]F^- were synthesized by the Department of Nuclear Medicine, Zhongshan Hospital, Fudan University. KA was purchased from Sigma−Aldrich LLC. (USA). The anti-TSPO antibody was purchased from Abcam Co., Ltd. (UK). Fluorescein isothiocyanate (FITC)-conjugated goat anti-rabbit IgG, anti-CD68 rabbit antibody, and anti-GFAP rabbit antibody were purchased from Servicebio Technology Co., Ltd. (China). The anti-TSPO rabbit antibody was purchased from Thermo Fisher Scientific Inc. (USA). The Nissl staining solution was purchased from Beyotime Biotech. Inc. (China). A fluorine multifunctional module was purchased from Sumitomo Corporation (Japan). QMA and C-18 Sep-Pak cartridges and C-18 column for analytical HPLC were purchased from Waters Corporation (USA). C-18 column for preparative HPLC was purchased from Agilent Technologies, Inc. (USA). A CRC-25R radionuclide activity meter was purchased from Capintec. Inc. (USA). GC1200 γ radioimmunoassay counter was purchased from Anhui USTC Zonkia Scientific Instruments Co., Ltd. (China). Micro PET/CT was purchased from Siemens Ltd. (German). A CR 35 BIO imaging system was purchased from Dürr India Private Ltd. (India). RAW 264.7 cells were purchased from Zhong Qiao Xin Zhou Biotechnology Co., Ltd. (China). ICR mice (6−8 weeks old, 25−30 g) and SD rats (8−9 weeks old, 250−300 g) were purchased from Beijing Vital River Laboratory Animal Technology Co., Ltd. (China).

4.2. Chemistry

All chemical reagents and solvents obtained from commercial companies were not further purified during use, except for the notes. Chemical reactions were performed following the standard procedures. The reactions were detected using HPLC or thin-layer chromatography (TLC). The purity of the target compounds was ≥95%. Compounds were characterized by ^{1}H, ^{13}C, and ^{19}F NMR or ESI-MS; the results are outlined in the Supporting Information Figs. S1−S19.

4.2.1. General procedure for the synthesis of Pre-CF_3-1

Synthesis of 2-amino-N-methoxy-N-methylbenzamide (Pre-CF_3-1). A mixture of isatoic anhydride (16.70 g, 102.37 mmol), *N*,*O*-dimethylhydroxylamine hydrochloride (DMHH, 11.00 g, 112.77 mmol), 4-dimethylaminopyridine (DMAP, 1.30 g, 10.64 mmol), triethylamine (Et_3N, 15.75 mL, 112.94 mmol), and acetonitrile (ACN, 80 mL) in a 500-mL single-necked vial was at room temperature (RT) for 24 h. Liquid chromatography-mass spectrometry (LC−MS) confirmed the complete consumption of the starting materials. Water (200 mL) was added to the reaction mixture to quench the reaction. After extraction with ethyl acetate (EA, 150 mL × 3), the mixture was washed with water and brine and dried over $NaSO_4$. The organic phase was concentrated and purified through column chromatography (petroleum ether (PE): EA = 1:1) to obtain Pre-CF_3-1 as a yellow oil (15.00 g, 83.24 mmol, 81.31% yield). ^{1}H NMR (300 MHz, $CDCl_3$): δ 3.35 (s, 3H), 3.60 (s, 3H), 4.66 (s, 2H), 6.67−6.72 (m, 2H), 7.16−7.21 (m, 1H), 7.34−7.38 (s, 1H) (Fig. S1).

4.2.2. General procedure for the synthesis of precursor Br-CF_2-QC

Step 1: Synthesis of (2-aminophenyl) (m-tolyl)methanone (Pre-CF_3-2). Under N_2 protection, 3-bromotoluene (13.30 g, 77.76 mmol) was added to a 500-mL three-necked flask, followed by the addition of tetrahydrofuran (THF, 100 mL). After cooling to −78 °C, *n*-butyllithium (*n*-BuLi, 77.70 mL, 155.40 mmol) was gradually added, and the mixture was stirred for 1 h. Then, a solution of Pre-CF_3-1 (14.00 g, 77.69 mmol) in THF (100 mL) was gradually added dropwise within about 30 min. The mixture was stirred at RT for 24 h. LC−MS confirmed the complete consumption of the starting materials. Ethyl alcohol (EtOH, 1 mL) was added to the reaction mixture to quench the reaction, followed by the addition of water (200 mL). After extraction with EA (200 mL × 3), the mixture was washed with water and brine and dried over $NaSO_4$. The organic phase was concentrated and purified through column chromatography (PE: EA = 5:1) to obtain Pre-CF_3-2 (7.30 g, 34.55 mmol, 44.47% yield). MS (ESI): calcd for $C_{14}H_{13}NO$ $[M]^+$, 211.1; found, 212.1 $[M + H]^+$ (Fig. S2).

Step 2: Synthesis of ethyl 4-(m-tolyl)quinazoline-2-carboxylate (Pre-CF_3-3). A mixture of Pre-CF_3-2 (7.00 g, 33.13 mmol), ethyl glyoxalate (3.40 g, 33.30 mmol), ammonium acetate (NH_4OAc, 2.60 g, 33.73 mmol), EtOH (45 mL), and H_2O (20 mL) was stirred in a 250-mL reaction flask at RT for 72 h. LC−MS confirmed the complete consumption of the starting materials. Water (100 mL) was then added to the reaction mixture to quench the reaction. After extraction with EA (50 mL × 3), the mixture was washed with water and brine and dried over $NaSO_4$. The organic phase was concentrated and purified through column chromatography (PE: EA = 5:1) to obtain Pre-CF_3-3 (3.60 g, 12.31 mmol, 37.16% yield). MS (ESI): calcd for $C_{18}H_{16}N_2O_2$ $[M]^+$, 292.1; found, 293.1 $[M + H]^+$ (Fig. S3). ^{1}H NMR (300 MHz, $CDCl_3$): δ 1.50 (t, 3H, J = 7.20 Hz), 2.48 (s, 3H), 4.61 (q, 2H, J = 7.20 Hz), 7.38−7.48 (m, 2H), 7.58−7.60 (m, 1H), 7.66−7.68 (m, 2H), 7.96−8.01 (m, 1H), 8.18−8.21 (m, 1H), 8.29−8.33 (m, 1H) (Fig. S4).

Step 3: Synthesis of 4-(m-tolyl)quinazoline-2-carboxylic acid (Pre-CF_3-4). A mixture of Pre-CF_3-3 (3.50 g, 11.97 mmol), NaOH (0.96 g, 24.00 mmol), and EtOH (40 mL) was stirred in a 100-mL three-necked flask at RT for 24 h. TLC analysis confirmed the

complete consumption of the starting materials. Water (50 mL) was added to the reaction mixture to quench the reaction. The reaction solution was concentrated to remove EtOH, hydrochloric acid (1 mol/L, 20 mL) was added, and the pH was adjusted to 1. After extraction with EA (40 mL × 3), the mixture was washed with water and brine and dried over $NaSO_4$. The organic phase was concentrated under reduced pressure to obtain the crude product Pre-CF_3-4 without purification (2.50 g, 9.46 mmol, 79.03%).

Step 4: Synthesis of 4-(m-tolyl)quinazoline-2-carbonyl chloride (Pre-CF_3-5). Under N_2 protection, Pre-CF_3-4 (2.30 g, 8.70 mmol), oxalyl chloride (OC, 2.20 g, 17.33 mmol), and dichloromethane (DCM, 25 mL) were added sequentially to a 100-mL three-necked flask, and *N*,*N*-dimethylformamide (DMF, 3 drops) was added dropwise. The mixture was stirred at RT for 24 h. TLC analysis confirmed the complete reaction of the starting materials. The reaction mixture was concentrated and then dried using an oil pump to obtain the crude product Pre-CF_3-5 without purification (1.82 g, 6.44 mmol, yield 74.02%).

Step 5: Synthesis of (R)-N-(sec-butyl)-4-(m-tolyl)quinazoline-2-carboxamide (Pre-CF_3-6). A mixture of Pre-CF_3-5 (1.80 g, 6.37 mmol), (*R*)-(−)-2-aminobutane (0.47 g, 6.43 mmol), Et_3N (1.94 g, 19.17 mmol), and DCM (20 mL) was stirred in a 100-mL three-necked flask at RT for 2 h. TLC analysis showed a complete reaction of the starting materials. Water (50 mL) was added to the reaction mixture to quench the reaction. After extraction with EA (40 mL × 3), the mixture was washed with water and brine and dried over $NaSO_4$. The mixture was purified through column chromatography (PE: EA = 3:1) to obtain Pre-CF_3-6 (1.75 g, 5.48 mmol, yield 86.03%). MS (ESI): calcd for $C_{20}H_{21}N_3O$ $[M]^+$, 319.2; found, 320.1 $[M + H]^+$ (Fig. S5). ^{1}H NMR (300 MHz, $CDCl_3$): δ 1.00 (t, 3H, J = 7.50 Hz), 1.26−1.31 (m, 3H), 1.63−1.68 (m, 2H), 2.50 (s, 3H), 4.22−4.30 (m, 1H), 7.41−7.55 (m, 2H), 7.57−7.71 (m, 3H), 7.94−7.99 (m, 1H), 8.15−8.18 (m, 2H), 8.31−8.35 (m, 1H) (Fig. S6).

Step 6: Synthesis of (R)-N-(sec-butyl)-N-methyl-4-(m-tolyl) quinazoline-2-carboxamide (Pre-CF_3-7). Under N_2 protection, Pre-CF_3-6 (1.70 g, 5.32 mmol) and THF (20 mL) were sequentially added to a 100-mL three-necked flask. After cooling to 0 °C, potassium tert-butoxide (*t*-BuOK, 1.80 g, 16.04 mmol) was added, and the mixture was stirred at 0 °C for 1 h. Then, CH_3I (0.91 g, 6.41 mmol) was slowly added, and the mixture was stirred at RT for 16 h. TLC analysis showed a complete reaction of the starting materials. Water (50 mL) was added to the reaction mixture to quench the reaction. After extraction with EA (25 mL × 3), the mixture was washed with water and brine and dried over $NaSO_4$. The organic phase was concentrated and purified through column chromatography (PE: EA = 3:1) to obtain Pre-CF_3-7 (1.14 g, 3.42 mmol, yield 64.29%). MS (ESI): calcd for $C_{21}H_{23}N_3O$ $[M]^+$, 333.2; found, 334.2 $[M + H]^+$ (Fig. S7).

Step 7: Synthesis of (R)-4-(3-(bromomethyl)phenyl)-N-(sec-butyl)-N-methylquinazoline-2-carboxamide (Pre-CF_3-8). A mixture of Pre-CF_3-7 (1.10 g, 3.30 mmol), *N*-bromosuccinimide (NBS, 0.71 g, 3.99 mmol), 2,2′-azobis(2-methylpropionitrile) (AIBN, 0.16 g, 0.97 mmol), and 1,2-dichloroethane (DCE, 15 mL) was heated to 80 °C in a 50-mL three-necked flask for 16 h. LC−MS showed that the desired compound was formed. The mixture was concentrated to dryness, and the crude product Pre-CF_3-8 was obtained without purification (0.72 g, 1.75 mmol, yield 53.03%). MS (ESI): calcd for $C_{21}H_{22}BrN_3O$ $[M]^+$, 411.1; found, 412.1 $[M + H]^+$ (Fig. S8).

Step 8: Synthesis of (R)-N-(sec-butyl)-N-methyl-4-(3-(((trifluoromethyl)sulfonyl)methyl)phenyl)quinazoline-2-carboxamide (Pre-CF_3-9). A mixture of Pre-CF_3-8 (0.70 g, 1.70 mmol), sodium trifluoromethanesulfinate (CF_3SO_2Na, 0.27 g, 1.73 mmol), and ACN (15 mL) was heated to 80 °C in a 50-mL three-necked flask for 16 h. LC−MS confirmed the complete consumption of the starting materials. Water (20 mL) was then added to the reaction mixture to quench the reaction. After extraction with EA (25 mL × 3), the mixture was washed with water and brine and dried over $NaSO_4$. The mixture was concentrated and purified through column chromatography (PE: EA = 2:1) to obtain Pre-CF_3-9 (0.67 g, 1.44 mmol, yield 84.71%). MS (ESI): calcd for $C_{22}H_{22}F_3N_3O_3S$ $[M]^+$, 465.1; found, 466.1 $[M + H]^+$ (Fig. S9).

Step 9: Synthesis of (R)-N-(sec-butyl)-4-(3-(difluoro((trifluoromethyl)sulfonyl)methyl)phenyl)-N-methylquinazoline-2-carboxamide (Pre-CF_2-QC). A mixture of Pre-CF_3-9 (0.60 g, 1.29 mmol), *N*-fluorobenzenesulfonimide (NFSI, 0.83 g, 2.63 mmol), K_3PO_4 (0.83 g, 3.91 mmol), and DMF (15 mL) was stirred in a 50-mL three-necked flask at RT for 16 h. LC−MS confirmed the complete consumption of the starting materials. Water (20 mL) was then added to the reaction mixture to quench the reaction. After extraction with EA (20 mL × 3), the mixture was washed with water and brine and dried over $NaSO_4$. The organic phase was concentrated and purified through column chromatography (PE: EA = 2:1) to obtain Pre-CF_2-QC (0.23 g, 0.46 mmol, 35.66% yield). MS (ESI): calcd for $C_{22}H_{20}F_5N_3O_3S$ $[M]^+$, 501.1; found, 502.1 $[M + H]^+$ (Fig. S10). ^{1}H NMR (300 MHz, $CDCl_3$): δ 0.88 & 1.04 (t, 3H, J = 7.50 Hz), 1.24−1.29 (m, 3H), 1.37−1.76 (m, 2H), 2.84 & 3.04 (s, 3H), 3.54 & 4.89 (m, 1H), 7.69−7.74 (m, 1H), 7.80−7.85 (m, 1H), 7.93−8.02 (m, 2H), 8.06−8.11 (m, 1H), 8.15−8.22 (m, 3H) (Fig. S11). ^{19}F NMR (282 MHz, $CDCl_3$): δ −69.78 (m, 3F), −98.64 (m, 2F) (Fig. S12).

Step 10: Synthesis of (R)-4-(3-(bromodifluoromethyl)phenyl)-N-(sec-butyl)-N-methylquinazoline-2-carboxamide (Br-CF_2-QC). A mixture of Pre-CF_2-QC (0.20 g, 0.40 mmol), LiBr (0.17 mg, 2.00 mmol), and ACN (30 mL) was stirred in a 50-mL three-necked flask at 80 °C for 16 h. LC−MS confirmed the complete consumption of the starting materials. Water (20 mL) was then added to the reaction mixture to quench the reaction. After extraction with EA (30 mL × 3), the mixture was washed with water and brine and dried over $NaSO_4$. The organic phase was concentrated and purified through column chromatography (*n*-hexane (Hex): EA = 1:1) to obtain Br-CF_2-QC (0.10 g, 0.22 mmol, 55.00% yield). MS (ESI) of Br-CF_2-QC. MS: calcd for $C_{21}H_{20}BrF_2N_3O$ $[M]^+$, 447.1; found, 448.1 $[M + H]^+$ (Fig. S13). ^{1}H NMR of Br-CF_2-QC. ^{1}H NMR (300 MHz, $CDCl_3$): δ 0.88 & 1.04 (t, 3H, J = 7.50 Hz), 1.25−1.29 (m, 3H), 1.40−1.76 (m, 2H), 2.83 & 3.04 (s, 3H), 3.57 & 4.85 (m, 1H), 7.67−7.72 (m, 2H), 7.82−7.84 (m, 1H), 7.93−8.00 (m, 2H), 8.05−8.10 (m, 2H), 8.17−8.20 (m, 1H) (Fig. S14). ^{19}F NMR of Br-CF_2-QC. ^{19}F NMR (282 MHz, $CDCl_3$): δ −43.96 & −43.997 (Fig. S15).

4.2.3. General procedure for the synthesis of [^{19}F]F-TFQC

*Step 1: Synthesis of (2-aminophenyl) (3-(trifluoromethyl)phenyl) methanone (compound **1**).* 3-Bromobenzotrifluoride (866.49 mg, 3.87 mmol) and THF were added to a three-necked vial. After cooling to −78 °C, *n*-BuLi (17.5 mL, 7.78 mmol) was slowly added and stirred for 30 min. Then, a solution of Pre-CF_3-1 (697.00 mg, 3.87 mmol) in THF was gradually added dropwise,

and the mixture was at −30 °C for 2 h. EtOH (1 mL) was added to the reaction mixture to quench the reaction, followed by the addition of 50 mL of water. After extraction with DCM (50 mL × 3), the mixture was washed with water and brine and dried over $NaSO_4$. The organic phase was concentrated and purified through column chromatography (PE: EA = 5:1) to obtain compound **1** as a light yellow solid (228.11 mg, 0.86 mmol, 22.22%). ^{1}H NMR (300 MHz, $CDCl_3$): δ 6.20 (s, 3H), 6.62−6.65 (m, 1H), 6.77−6.80 (m, 1H), 7.33−7.40 (m, 2H), 7.61−7.66 (m, 1H), 7.81−7.86 (m, 2H), 7.93 (s, 1H) (Fig. S16).

*Step 2: Synthesis of ethyl 4-(3-(trifluoromethyl)phenyl)quinazoline-2-carboxylate (compound **2**).* A mixture of compound **1** (228.11 mg, 0.86 mmol), ethyl glyoxalate (87.80 mg, 0.86 mmol), EtOH (15 mL), NH_4OAc (198.66 mL, 2.58 mmol), and H_2O (5 mL) in a 100-mL single-necked vial was maintained at RT for 3 days. Water (50 mL) was added to the reaction mixture to quench the reaction. After extraction with DCM (50 mL × 3), the mixture was washed with water and brine and dried over $NaSO_4$. Then, the mixture was rotary evaporated and purified through column chromatography (PE: EA = 5:1) to obtain compound **2** as a light yellow solid (68.00 mg, 0.20 mmol, 23.26%). ^{1}H NMR (300 MHz, $CDCl_3$): δ 1.54 (t, 3H, J = 7.20 Hz), 4.62 (q, 2H, J = 7.20 Hz), 7.71−7.77 (m, 2H), 7.85−7.87 (m, 1H), 8.01−8.11 (m, 4H), 8.36−8.39 (m, 1H) (Fig. S17).

Step 3: Synthesis of N-((2R)-but-2-yl)-N-methyl-4-(3-(trifluoromethyl)phenyl)quinazoline-2-carboxamide ([^{19}F]F-TFQC). A mixture of trimethylaluminium (0.63 mL, 0.48 mmol), (*R*)-(−)-2-aminobutane (35.00 mg, 0.48 mmol), and DCE (15 mL) in a three-necked vial was stirred at RT for 30 min. Then, compound **2** in DCE was added and reacted at 80 °C for 2 h. The organic phase was rotary evaporated and purified through column chromatography (Hex: EA = 1:1) to obtain [^{19}F]F-TFQC as a light yellow solid (38.00 mg, 0.10 mmol, 50.00%). MS (ESI): calcd for $C_{21}H_{20}F_3N_3O$ $[M + H]^+$, 387.1558; found, 388.1609. ^{13}C NMR (151 MHz, $CDCl_3$): δ 9.99 & 10.02, 16.19 & 17.43, 24.76 & 26.19, 25.60 & 28.77, 49.04 & 54.77, 121.03 & 121.06, 122.81 (q, J = 270.5 Hz),125.34 & 125.37, 125.90 (q, J = 3.3 Hz), 125.99 (q, J = 3.8 Hz), 127.73, 128.18 & 128.21, 128.45 & 128.52, 130.23 (q, J = 33 Hz), 132.39 & 132.49, 133.43, 136.50, 150.15 & 150.23, 157.69, 166.33, 166.51 & 166.57 (Fig. S18). ^{1}H NMR (600 MHz, $CDCl_3$): δ 0.81 & 0.97 (t, 3H, J = 7.50 Hz), 1.18−1,21 (m, 3H), 1.34−1.67 (m, 2H), 2.76 & 2.97 (s, 3H), 3.50 & 4.78 (m, 1H), 7.61−7.66 (m, 2H), 7.78 (d, 1H, J = 7.80 Hz), 7.90−7.95 (m, 2H), 7.98−8.02 (m, 2H), 8.11−8.14 (m, 1H). ^{19}F NMR (565 MHz, $CDCl_3$): δ −62.56 & −62.63 (Fig. S19).

4.3. Radiochemistry

[^{18}F]F-TFQC was synthesized using a fluorine multifunctional module. Cyclotron-produced [^{18}F]F^- was trapped on a QMA Sep-Pak cartridge and eluted out with a mixed solution of tetraethylammonium bromide (TEAB, 40 mg/mL, 0.5 mL) and ACN (0.5 mL), and then dried with ACN (1.0 mL) twice under N_2 at 120 and 100 °C respectively. A solution of Br-CF_2-QC (~5 mg) in ACN (1.0 mL) was added to a sealed reaction vial containing the dried [^{18}F]F^-, and then heated at 120 °C for 15 min. The mixture was pre-purified with a C-18 Sep-Pak cartridge and then isolated through the reversed-phase preparative HPLC (column: 5 μm, 9.4 × 250 mm; mobile phase: 6.0/4.0 (*v*/*v*) ACN/H_2O containing 0.1% trifluoroacetic acid (TFA); flow rate: 3 mL/min). The solution was then diluted with distilled water (20 mL) and then passed through another C-18 Sep-Pak cartridge. The C-18 Sep-Pak cartridge was washed with distilled water (10 mL × 2), and the product was eluted with EtOH (1 mL) into a sterile vial. The product solution was diluted to 10% EtOH with NS for subsequent cell and animal experiments. The RCY of [^{18}F]F-TFQC was calculated by measuring the activity of the final product using a CRC-25R radionuclide activity meter, which was decay-corrected to the EOS. The RCP and identification of [^{18}F]F-TFQC were performed by co-injection with [^{19}F]F-TFQC using an analytical HPLC system (column: 3.5 μm, 4.6 mm × 100 mm; mobile phase: 5.5/4.5 (*v*/*v*) ACN/H_2O containing 0.1% TFA for 15 min; flow rate: 1 mL/min). The specific activity (EOS) was determined using an ultraviolet (UV) calibration curve (λ = 254 nm).

4.4. In vitro stability, in vivo stability, and octanol/water partition coefficient

The *in vitro* stability assay was performed using both a mixture of [^{18}F]F-TFQC and NS and a mixture of [^{18}F]F-TFQC and 1% BSA at 37 °C. These two mixtures were subjected to HPLC analysis after 1, 2, 4, and 6 h.

Healthy SD rats were used to evaluate the *in vivo* stability. After the anesthesia with 1.5%−2.0% isoflurane/oxygen, SD rats were intravenously administrated with [^{18}F]F-TFQC (80−100 MBq/400 μL) and sacrificed at 5, 30, and 60 min post injection. Then, brains were removed, and 0.01 mol/L phosphate buffer saline (PBS, pH 7.4) containing the protease inhibitor was added for homogenization. The radioactive supernatant from the homogenized brain was separated by centrifugation at 10,000 rpm for 5 min and thoroughly mixed with ice-cold ACN. The supernatant of the ACN mixture was collected by centrifugation at 10,000 rpm for 5 min. After 0.22-μm filtering, the radioactive supernatant was subjected to HPLC analysis.

For the octanol/water partition coefficient study, [^{18}F]F-TFQC (0.37 MBq/10 μL) was added to a mixture of n-octanol (500 μL) and 0.01 mol/L PBS (500 μL) and vortexed for 2 min at RT, followed by centrifugation at 5000 rpm for 3 min. Samples (10 μL) were obtained from the n-octanol and 0.01 mol/L PBS layers, and the radioactivity of the samples was measured using a GC1200 γ radioimmunoassay counter. The octanol/water partition coefficient (log*D*) was calculated as Eq. (1):

$$\text{Log}D = \text{Log}(n\text{-octanol counts/aqueous phase counts}) \quad (1)$$

4.5. Cell culture and ICC

RAW 264.7 cells were cultured in RPMI 1640 medium containing 10% fetal bovine serum and 1% penicillin-streptomycin solution. The cells were kept at 37 °C in a humidified atmosphere with 5% CO_2. For the ICC experiment, cells (1×10^4 cells/well) were seeded in 24-well plates overnight and divided into experimental and no primary antibody control groups. The cells were fixed with 4% paraformaldehyde at 4 °C for 10 min and permeabilized with 0.3% Triton X-100 at RT for 5 min, followed by blocking with 5% BSA at RT for 1 h. Then, an anti-TSPO antibody (1:125) was added to the cells in the experimental group but not to those in the no primary antibody control group. The cells were initially incubated overnight at 4 °C followed by further incubation at RT for 1 h with FITC-conjugated goat anti-rabbit IgG (1:200). Nuclear DNA was labeled blue with 4′,6-diamidino-2-phenylindole (DAPI). The images were acquired using an Olympus imaging system.

4.6. In vitro cell binding

RAW 264.7 cells (2×10^4 cells/well) were plated in 24-well plates 1 day before the experiment. The wells were then divided into two groups. The cells in Group 1 were pre-saturated with 344.53 nmol/L [^{19}F]F-TFQC for 30 min, while those in Group 2 were not treated. Then, all cells were incubated with 0.2 nmol/L [^{18}F]F-TFQC for 15 min, 30 min, 1 and 2 h at 37 °C. For the total binding assay, the cells (2×10^4 cells/well) were plated in 24-well plates 1 day before the experiment. All cells were incubated with equally diluted (0.2−400 nmol/L) [^{18}F]F-TFQC for 2 h at 37 °C. For both experiments, the medium and 0.01 mol/L PBS used for washing were collected as supernatants, and the cells lysed with NaOH (1 mol/L) were collected as precipitates. The radioactivity of the supernatants and precipitates was measured using a γ counter. The maximum binding ability (B_{max}) and dissociation constant (K_d) were calculated using GraphPad Prism 9.0 with a "One site-Total" model.

4.7. Biosafety

To evaluate the toxicity of [^{18}F]F-TFQC, 24 healthy mice were divided into four groups, with each group comprising three male mice and three female mice. These mice received intravenous NS (100 μL) or low-dose (3.7 MBq/0.1 nmol/100 μL), medium-dose (18.5 MBq/0.5 nmol/100 μL) and high-dose (37 MBq/1.0 nmol/100 μL) of [^{18}F]F-TFQC, followed by measurement of the body weight at 1, 2, 3, 4, 5, 6, 7, 14, 21, and 28 days post injection. At the end of the observation period, fresh blood was collected from the mice for hematological examinations, including blood routine (WBC, RBC, and PLT), liver function (ALT, AST, and ALB), and kidney function (UREA, CREA, and UA) tests. Finally, the major organs, including the heart, liver, spleen, lung, kidney, stomach, intestine, bone, muscle, and brain, were collected from the mice for H&E staining.

4.8. Pharmacokinetics and biodistribution

The pharmacokinetic profile of [^{18}F]F-TFQC was evaluated in three healthy mice that had been intravenously injected with [^{18}F]F-TFQC (3.7 MBq/100 μL). Blood samples from the tail vein were collected with a capillary pipette (5−10 μL) and weighed at 1, 3, 5, 10, 15, 30 min, 1, 1.5, 2, 3, and 4 h post injection. Subsequently, the radioactivity was measured using a γ counter, and the results were expressed as counts per minute (CPM) following a decay correction. Moreover, the blood half-life of [^{18}F]F-TFQC was calculated by GraphPad Prism 9.0 using a "Two phase decay" model and expressed as the percentage of injected dose per gram (% ID/g) using Eq. (2):

$$\%\ \text{ID/g} = [(\text{Blood CPM/injected CPM})/\text{grams of blood}] \times 100 \quad (2)$$

Twenty-one healthy mice (n = 3/group) were intravenously injected with [^{18}F]F-TFQC (3.7 MBq/100 μL) to determine the biodistribution properties. The mice were sacrificed at 15, 30 min, 1, 1.5, 2, 3, and 4 h post injection, and the organs (blood, heart, liver, spleen, lung, kidney, stomach, intestine, skeleton, muscle, and brain) were harvested and weighed. The CPM was obtained as previously described. Organ activity was expressed as % ID/g using Eq. (3):

$$\%\ \text{ID/g} = [(\text{Organs CPM/injected CPM})/\text{grams of organs}] \times 100 \quad (3)$$

4.9. KA-induced epileptic rat models

The rats were randomly divided into the epilepsy and sham groups. The rats were deeply anesthetized through an intraperitoneal injection of 2% pentobarbital (0.3 mL/100 g) and placed in a stereotaxic device. The epilepsy group was intrahippocampally injected with KA (1.0 μg/1.0 μL; AP: −3.1 mm, ML: −1.8 mm, DV: −3.0 mm), while the sham group was injected with an equal volume of NS. The behaviors of the rats were monitored by video recording. The behavioral manifestations of seizures in the rat models were scored as follows based on the Racine's scale[41]: 0, no motor seizure activity; I, eye closure and masticatory movements; II, head nodding; III, forelimb clonus; IV, clonus with rearing; and V, clonus with rearing and falling. Epileptic rats with seizure grades of IV−V were selected for subsequent experiments.

4.10. Micro PET/CT imaging procedures

[^{18}F]F-TFQC PET was performed at 1 day, 1 week, and 1 month after KA or NS injection. All imaging procedures were performed under isoflurane anesthesia (1.5%−2.0% with oxygen). After an intravenous bolus injection of [^{18}F]F-TFQC (~37.0 MBq) via the tail vein, a 60-min dynamic PET scan was immediately performed (16 frames: 4 × 30, 8 × 60, 1 × 300, and 3 × 900 s), followed by a 10-min CT scan. For the blocked study, 2 mg/kg [^{19}F]F-TFQC was injected intravenously into the epileptic rats via the tail vein 10 min before [^{18}F]F-TFQC injection. The images were reconstructed using the 3D ordered subset expected maximum algorithm in the Siemens Inveon software. PET images were fused with an MRI template using the "CoRegistration Preprocessing" of PMOD 3.2 software. The VOIs of the "Hippocampus" (*i.e.*, EZ) and "CaudatePutmen" (reference area) were outlined accurately based on the rat (W. Schiffer) atlas of PMOD 3.2 software, and the SUV_{mean} was generated. The TACs were used to observe radioactivity changes in the brain over time. The T/NT (ratio of $SUV_{mean(Hippocampus)}$ to $SUV_{mean(CaudatePutmen)}$) values were calculated for semi-quantitative analysis.

4.11. In vitro autoradiography

After anesthetizing the rats with 3% sodium pentobarbital (0.1−0.2 mL/100 g) and transcardially perfused with 4 °C NS, the brains were harvested and embedded with OCT. Continuous coronal slices (20 μm thick) were prepared using a frozen microtome. Frozen brain sections were pre-incubated in Tris buffer A (50 mmol/L, pH 7.4, RT) containing 5% BSA for 20 min. Then, the pre-incubated brain slices were divided into three groups and incubated with 14.5 nmol/L [^{18}F]F-TFQC, a mixture of 14.5 nmol/L [^{18}F]F-TFQC and 14.17 μmol/L PK11195, and a mixture of 14.5 nmol/L [^{18}F]F-TFQC and 12.91 μmol/L [^{19}F]F-TFQC for 45 min. Following incubation, the brain sections were washed with Tris buffer B (50 mmol/L, pH 7.4, 4 °C) twice for 5 min each time and then dipped in distilled water for 30 s. The brain sections were air-dried and placed on the IP plate in the dark overnight. The IP plate was scanned at a pixel size of 25 μm resolution using a CR 35 BIO imaging system, and obtained images were analyzed by ImageJ.

4.12. Nissl staining and IHF

The frozen brain sections were used for Nissl staining and IHF analysis. Nissl staining was performed according to the manufacturer's instructions. For IHF staining, slices were incubated

with primary antibodies, including anti-CD68 rabbit antibody (1:200), anti-GFAP rabbit antibody (1:500), and anti-TSPO rabbit antibody (1:100), at 4 °C overnight and with secondary antibodies at RT for 1 h. DAPI staining was also conducted to visualize the nuclei. All images were analyzed using the ImageJ software.

4.13. *Statistical analysis*

All data are expressed as the mean ± standard deviation unless otherwise stated. Paired *t*-test and independent sample *t*-test were used for two-group comparisons. A P value of <0.05 was considered significant. Statistical analyses were performed using GraphPad Prism 9.0 and IBM SPSS 20.0.

Acknowledgments

This work was supported by the National Natural Science Foundation of China (No. 82172002 and 82272058, China), Shanghai Municipal Science and Technology Committee of Shanghai Outstanding Academic Leaders Plan (No. 21XD1423500, China), and National Key Research and Development Program of China (No. 2022YFC2406901). We also thank Bin Ji, Xiyan Rui, and Xinran Zhao from School of Pharmacy, Fudan University for the autoradiography apparatus, and Ruimin Huang and Xiaoyu Zhou from Shanghai Institute of Materia Medica Chinese Academy of Sciences for the micro PET/CT.

Author contributions

Wenhui Fu: Conceptualization, Data curation, Formal analysis, Investigation, Methodology, Writing − original draft. Qingyu Lin: Formal analysis, Funding acquisition, Methodology, Writing − review & editing. Zhequan Fu: Conceptualization, Methodology. Tingting Yang: Data curation, Methodology. Dai Shi: Data curation, Methodology. Pengcheng Ma: Data curation, Methodology. Hongxing Su: Data curation, Methodology. Yunze Wang: Data curation, Methodology. Guobing Liu: Conceptualization, Methodology. Jing Ding: Methodology, Supervision. Hongcheng Shi: Supervision, Writing − review & editing. Dengfeng Cheng: Conceptualization, Funding acquisition, Supervision, Writing − review & editing.

Conflicts of interest

The authors declare no competing financial interests.

Appendix A. Supporting information

Supporting information to this article can be found online at https://doi.org/10.1016/j.apsb.2024.05.031.

References

1. Vezzani A, French J, Bartfai T, Baram TZ. The role of inflammation in epilepsy. *Nat Rev Neurol* 2011;**7**:31−40.
2. Yao R, Pan R, Shang C, Li X, Cheng J, Xu J, et al. Translocator protein 18 kDa (TSPO) deficiency inhibits microglial activation and impairs mitochondrial function. *Front Pharmacol* 2020;**11**:986.
3. Chen MK, Guilarte TR. Translocator protein 18 kDa (TSPO): molecular sensor of brain injury and repair. *Pharmacol Ther* 2008;**118**:1−17.
4. Parente A, Feltes PK, Vállez García D, Sijbesma JW, Moriguchi Jeckel CM, Dierckx RA, et al. Pharmacokinetic analysis of ^{11}C-PBR28 in the rat model of herpes encephalitis: comparison with (*R*)-^{11}C-PK11195. *J Nucl Med* 2016;**57**:785−91.
5. Owen DR, Yeo AJ, Gunn RN, Song K, Wadsworth G, Lewis A, et al. An 18-kDa translocator protein (TSPO) polymorphism explains differences in binding affinity of the PET radioligand PBR28. *J Cereb Blood Flow Metab* 2012;**32**:1−5.
6. Fan Z, Harold D, Pasqualetti G, Williams J, Brooks DJ, Edison P. Can studies of neuroinflammation in a TSPO genetic subgroup (HAB or MAB) be applied to the entire AD cohort. *J Nucl Med* 2015;**56**:707−13.
7. Downer OM, Marcus R, Zürcher NR, Hooker JM. Tracing the history of the human translocator protein to recent neurodegenerative and psychiatric imaging. *ACS Chem Neurosci* 2020;**11**:2192−200.
8. Zanotti-Fregonara P, Pascual B, Rizzo G, Yu M, Pal N, Beers D, et al. Head-to-head comparison of ^{11}C-PBR28 and ^{18}F-GE180 for quantification of the translocator protein in the human brain. *J Nucl Med* 2018;**59**:1260−6.
9. Ramakrishnan NK, Hird M, Thompson S, Williamson DJ, Qiao L, Owen DR, et al. Preclinical evaluation of (*S*)-[^{18}F]GE387, a novel 18-kDa translocator protein (TSPO) PET radioligand with low binding sensitivity to human polymorphism rs6971. *Eur J Nucl Med Mol Imaging* 2021;**49**:125−36.
10. Qiao L, Fisher E, McMurray L, Milicevic Sephton S, Hird M, Kuzhuppilly-Ramakrishnan N, et al. Radiosynthesis of (*R,S*)-[^{18}F]GE387: a potential PET radiotracer for imaging translocator protein 18 kDa (TSPO) with low binding sensitivity to the human gene polymorphism rs6971. *ChemMedChem* 2019;**14**:982−93.
11. Perrone M, Moon BS, Park HS, Laquintana V, Jung JH, Cutrignelli A, et al. A novel PET imaging probe for the detection and monitoring of translocator protein 18 kDa expression in pathological disorders. *Sci Rep* 2016;**6**:20422.
12. Lee SH, Denora N, Laquintana V, Mangiatordi GF, Lopedota A, Lopalco A, et al. Radiosynthesis and characterization of [^{18}F]BS224: a next-generation TSPO PET ligand insensitive to the rs6971 polymorphism. *Eur J Nucl Med Mol Imaging* 2021;**49**:110−24.
13. Tiwari AK, Ji B, Yui J, Fujinaga M, Yamasaki T, Xie L, et al. [^{18}F]FEBMP: positron emission tomography imaging of TSPO in a model of neuroinflammation in rats, and *in vitro* autoradiograms of the human brain. *Theranostics* 2015;**5**:961−9.
14. Ji B, Ono M, Yamasaki T, Fujinaga M, Zhang MR, Seki C, et al. Detection of Alzheimer's disease-related neuroinflammation by a PET ligand selective for glial *versus* vascular translocator protein. *J Cereb Blood Flow Metab* 2021;**41**:2076−89.
15. MacAskill MG, Stadulyte A, Williams L, Morgan T, Sloan NL, Alcaide-Corral CJ, et al. Quantification of macrophage-driven inflammation during myocardial infarction with ^{18}F-LW223, a novel TSPO radiotracer with binding independent of the rs6971 human polymorphism. *J Nucl Med* 2021;**62**:536−44.
16. Kreisl WC, Kim MJ, Coughlin JM, Henter ID, Owen DR, Innis RB. PET imaging of neuroinflammation in neurological disorders. *Lancet Neurol* 2020;**19**:940−50.
17. Ikawa M, Lohith TG, Shrestha S, Telu S, Zoghbi SS, Castellano S, et al. ^{11}C-ER176, a radioligand for 18-kDa translocator protein, has adequate sensitivity to robustly image all three affinity genotypes in human brain. *J Nucl Med* 2017;**58**:320−5.
18. Chen H, Jiang Z, Cheng X, Zheng W, Sun Y, Yu Z, et al. [^{18}F]BIBD-239: ^{18}F-labeled ER176, a positron emission tomography tracer specific for the translocator protein. *Mol Pharm* 2022;**19**:2351−66.
19. Lee JH, Siméon FG, Liow JS, Morse CL, Gladding RL, Santamaria J, et al. *In vivo* evaluation of 6 analogs of ^{11}C-ER176 as candidate ^{18}F-labeled radioligands for 18-kDa translocator protein. *J Nucl Med* 2022;**63**:1252−8.
20. Siméon FG, Lee JH, Morse CL, Stukes I, Zoghbi SS, Manly LS, et al. Synthesis and screening in mice of fluorine-containing PET radioligands for TSPO: discovery of a promising ^{18}F-labeled ligand. *J Med Chem* 2021;**64**:16731−45.

21. Yang RY, Gao X, Gong K, Wang J, Zeng X, Wang M, et al. Synthesis of $ArCF_2X$ and [^{18}F]Ar-CF_3 *via* cleavage of the trifluoromethylsulfonyl group. *Org Lett* 2022;**24**:164−8.
22. Mizuta S, Stenhagen IS, O'Duill M, Wolstenhulme J, Kirjavainen AK, Forsback SJ, et al. Catalytic decarboxylative fluorination for the synthesis of tri- and difluoromethyl arenes. *Org Lett* 2013;**15**:2648−51.
23. van der Born D, Sewing C, Herscheid JK, Windhorst AD, Orru RV, Vugts DJ. A universal procedure for the [^{18}F]trifluoromethylation of aryl iodides and aryl boronic acids with highly improved specific activity. *Angew Chem Int Ed Engl* 2014;**53**:11046−50.
24. Ivashkin P, Lemonnier G, Cousin J, Grégoire V, Labar D, Jubault P, et al. [^{18}F]$CuCF_3$: a [^{18}F]trifluoromethylating agent for arylboronic acids and aryl iodides. *Chemistry* 2014;**20**:9514−8.
25. Kee CW, Tack O, Guibbal F, Wilson TC, Isenegger PG, Imiołek M, et al. ^{18}F-Trifluoromethanesulfinate enables direct C−H ^{18}F-trifluoromethylation of native aromatic residues in peptides. *J Am Chem Soc* 2020;**142**:1180−5.
26. Huiban M, Tredwell M, Mizuta S, Wan Z, Zhang X, Collier TL, et al. A broadly applicable [^{18}F]trifluoromethylation of aryl and heteroaryl iodides for PET imaging. *Nat Chem* 2013;**5**:941−4.
27. Fu Z, Lin Q, Hu B, Zhang Y, Chen W, Zhu J, et al. P2X7 PET radioligand ^{18}F-PTTP for differentiation of lung tumor from inflammation. *J Nucl Med* 2019;**60**:930−6.
28. Prabhakaran J, Underwood MD, Parsey RV, Arango V, Majo VJ, Simpson NR, et al. Synthesis and *in vivo* evaluation of [^{18}F]-4-[5-(4-methylphenyl)-3-(trifluoromethyl)-1*H*-pyrazol-1-yl]benzenesulfonamide as a PET imaging probe for COX-2 expression. *Bioorg Med Chem* 2007;**15**:1802−7.
29. Kilbourn MR, Pavia MR, Gregor VE. Synthesis of fluorine-18 labeled GABA uptake inhibitors. *Int J Rad Appl Instrum A* 1990;**41**:823−8.
30. Zhang S, Qiu Y, Huang L, Bi L, Guo Y, You K, et al. Ankylosing spondylitis PET imaging and quantifications *via* P2X7 receptor-targeting radioligand [^{18}F]GSK1482160. *Eur J Nucl Med Mol Imaging* 2023;**50**:3589−601.
31. Huang G, Lu X, Qiu Y, Bi L, Ye P, Yang M, et al. Hetero-aryl bromide precursor fluorine-18 radiosynthesis and preclinical evaluation of a novel positron emission tomography (PET) tracer [^{18}F]GSK1482160. *Bioorg Med Chem* 2022;**73**:116996.
32. Evens N, Muccioli GG, Houbrechts N, Lambert DM, Verbruggen AM, Van Laere K, et al. Synthesis and biological evaluation of carbon-11- and fluorine-18-labeled 2-oxoquinoline derivatives for type 2 cannabinoid receptor positron emission tomography imaging. *Nucl Med Biol* 2009;**36**:455−65.
33. Wang J, Sánchez-Roselló M, Aceña JL, del Pozo C, Sorochinsky AE, Fustero S, et al. Fluorine in pharmaceutical industry: fluorine-containing drugs introduced to the market in the last decade (2001−2011). *Chem Rev* 2014;**114**:2432−506.
34. Lévesque M, Avoli M. The kainic acid model of temporal lobe epilepsy. *Neurosci Biobehav Rev* 2013;**37**:2887−99.
35. Wang C, Zhang J, Song S, Li Z, Yin S, Duan W, et al. Imaging epileptic foci in mouse models *via* a low-density lipoprotein receptor-related protein-1 targeting strategy. *EBioMedicine* 2021;**63**:103156.
36. Rusina E, Bernard C, Williamson A. The kainic acid models of temporal lobe epilepsy. *eNeuro* 2021;**8**:ENEURO.0337-20.2021.
37. Garland EF, Dennett O, Lau LC, Chatelet DS, Bottlaender M, Nicoll J, et al. The mitochondrial protein TSPO in Alzheimer's disease: relation to the severity of AD pathology and the neuroinflammatory environment. *J Neuroinflammation* 2023;**20**:186.
38. Streng ML, Froula JM, Krook-Magnuson E. The cerebellum's understated role and influences in the epilepsies. *Neurobiol Dis* 2023;**183**:106160.
39. Remore LG, Rifi Z, Nariai H, Eliashiv DS, Fallah A, Edmonds BD, et al. Structural connections of the centromedian nucleus of thalamus and their relevance for neuromodulation in generalized drug-resistant epilepsy: insight from a tractography study. *Ther Adv Neurol Disord* 2023;**16**:17562864231202064.
40. Lanz B, Poitry-Yamate C, Gruetter R. Image-derived input function from the vena cava for ^{18}F-FDG PET studies in rats and mice. *J Nucl Med* 2014;**55**:1380−8.
41. Racine RJ. Modification of seizure activity by electrical stimulation. II. Motor seizure. *Electroencephalogr Clin Neurophysiol* 1972;**32**:281−94.